# Fastener behaviour in sheathed light-gauge steel stud walls under cyclic and monotonic actions

ORIGINAL ARTICLE

# Fastener behaviour in sheathed light-gauge steel stud walls under cyclic and monotonic actions

Nikolas Ringas[1], Yuner Huang[1], Jurgen Becque[2]

**Correspondence**

Dr. Yuner Huang
Lecturer
Institute for Infrastructure and Environment
School of Engineering
University of Edinburgh
Thomas Bayes Road, King's Buildings
EH9 3FG
Edinburgh, UK.
Email: Yuner.Huang@ed.ac.uk

**Abstract**

Steel framed buildings using digitally fabricated light-gauge steel sections, combined with an off-site panelised fabrication approach, are becoming more widespread and contribute towards reducing cost and erection time without requiring a large workforce to assemble them. Currently, design standards mandate the use of K- or X-bracing in these structures, thus neglecting the beneficial influence of the sheathing on the behaviour of the system, in particular its resistance to lateral loads. This composite behaviour is largely influenced by the performance of the fasteners, which may exhibit tilting, shear failure and fastener pull-out. This paper takes a first step towards accounting for composite action between light-gauge steel stud framing and calcium silicate board by focusing on the behaviour of the screws connecting both. Key failure modes are identified, based on direct pull-out tests and monotonic and cyclic connector shear tests. Significant pinching behaviour was observed under cyclic excitations.

**Keywords**

Calcium silicate board; cyclic loading; fastener behaviour; light-gauge steel; self-tapping screws; shear capacity.

## 1 Introduction

Construction methods using traditional materials, such as concrete and masonry, are characterised by labour-intensive activities, which significantly increase cost and delivery time. To tackle such limitations, part of the construction industry is gradually shifting towards the use of tailor-made solutions with prefabricated light-gauge steel (LGS) framing and sheathing panels, incorporating Modern Construction Methods (MCM) during fabrication. These systems produce light and sustainable structures that are easy to install [1]. This contributes to the minimisation of construction time, but also benefits efficiency and productivity. However, such frames usually require the installation of precisely cut K- or X- bracing members, which constitute a constrictive link in the fabrication and construction process and, consequently, impact on the delivery time of the structure.

The purpose of installing bracing is to increase the ability of the frame to resist lateral loading conditions (e.g. wind). However, previous research on composite framed wall systems has generated substantial evidence that the sheathing boards already act as diaphragms that significantly contribute to the lateral stiffness and capacity. Still, current European design standards disregard the influence of composite action arising from this arrangement, leading to conservatively designed structures characterised by excessive use of bracing. Additional research is therefore needed to gain increased knowledge and confidence in the behaviour of composite systems made up of LGS framing and sheathing boards, with the further purpose of developing accurate and safe design rules.

Some of the critical parameters in these composite systems affecting the behaviour and capacity have previously been identified to be the fastener arrangement and fastener geometry, the steel stud thickness, the sheathing thickness, the aspect ratio of the assembly and the energy absorption properties of the employed materials [2]–[6]. Multiple failure modes have also been identified in previous research, such as screw tilting, screw shear failure, screw pull-out and sheathing bearing failure [7]–[9].

In this article, a composite framing solution comprised of LGS and calcium silicate board (CSB) is examined as a construction method for low-rise multi-storey buildings. An emphasis was placed on the behaviour of the self-tapping screws that connect the two components. Pull out tests were conducted, as well as push out tests under monotonic and cyclic loading.

## 2 Description of the test program

The test specimens were designed based on typical LGS framed residential building assemblies found in Edinburgh, UK. The LGS studs consisted of a lipped channel section, made of S390GD+ZA steel, with a web height of 100 mm, a flange width of 45 mm and a lip length of 10 mm. The sheathing was made of 12 mm thick CSB,

1. School of Engineering, University of Edinburgh, Edinburgh, UK.
2. Department of Engineering, University of Cambridge, Cambridge, UK.

connected to the LGS studs using self-tapping screws with a diameter of 4.2 mm and a length of 38 mm at a spacing of 300 mm. A comprehensive series of tests, including material tests on both the CSB and the LGS, direct screw pull-out tests and monotonic and cyclic connector shear tests were carried out.

### 2.1 Material tests on light-gauge steel

The mechanical properties of S390GD+ZA cold-formed steel were determined through a series of tensile coupon tests. Longitudinal test specimens were extracted from flat unmachined sheets and from the webs and flanges of fabricated studs with a nominal thickness of 1.2 mm. The galvanized coating consisting of zinc and aluminium was removed by applying a 12 mol hydrochloric acid (HCl) solution to the surfaces of the coupons, to expose the virgin material and allow measurement of its thickness.

The coupons were tested using an Instron 4505 electro-mechanical universal testing machine (UTM) with a capacity of 100 kN. The longitudinal strain was recorded using a knife-edged extensometer with a gauge length of 50 mm. The test procedure and geometric properties of the coupons conformed to BS ISO 6892-1 [10]. The loading protocol applied a displacement rate of 0.40 mm/min until the peak load, followed by an increased rate of 1.0 mm/min until fracture. The test was halted for 3.5 minutes at a constant displacement once the yield plateau was reached, and near the ultimate strength, in order to eliminate the effect of the loading rate on the mechanical properties of the cold-formed steel [11]. These lower bound values were used in the determination of the mechanical properties of the material.

### 2.2 Material tests on calcium silicate boards

Since the material properties of CSB are different in tension and compression, separate experiments were conducted to determine its tensile and compressive properties. The tests were conducted using the same Instron 4505 UTM used for the LGS coupons.

Two tensile coupons were extracted from the CSB. The coupons were cut along the longitudinal direction of the CSB (i.e. the long direction of the board). Their geometry, as well as the loading protocol used in the tests, obeyed the ASTM D1037-12 rules [12], as illustrated in Figure 2(a). A constant loading rate of 0.25 mm/min was applied, while the strain was measured by a 50 mm extensometer, attached to the middle of the specimen.

Compressive coupons were extracted from the CSB in order to obtain its compressive mechanical properties in the directions normal and parallel to the faces. To examine the latter case, three test pieces measuring 75 mm in the longitudinal direction of the board, 102 mm in the transverse direction and 12 mm in thickness were extracted from a CSB, again in line with ASTM rules [12]. The three specimens were glued together using a two component LOCTITE EA 9466 epoxy adhesive and subsequently cut in three 25mm wide flat pieces, to form the compressive coupons, as illustrated in Figure 2(b). A constant displacement rate of 0.50 mm/min was applied until failure.

The compressive strength of the CSB in the direction normal to the surface (i.e. the through-thickness direction) was obtained by testing a specimen with a square 27 mm × 27 mm cross-section and a height of 12mm. The ultimate strength was measured at 5% deformation over the 12mm board nominal thickness, as prescribed by [13].

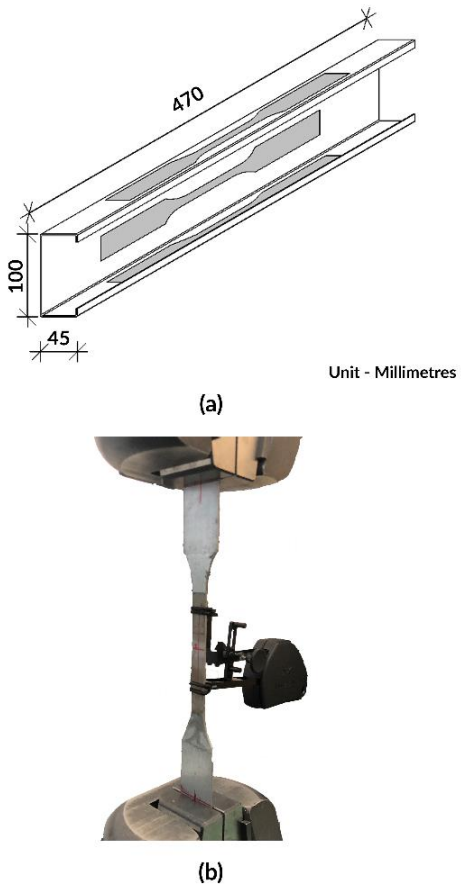


**Figure 1 –** Cold formed steel testing: (a) areas of coupon extraction, (b) test arrangement

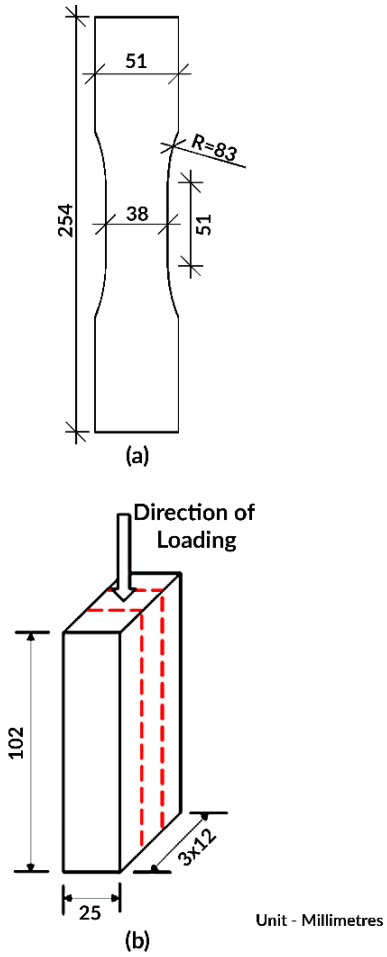


**Figure 2 –** Calcium Silicate: (a) Tensile coupon, (b) Compressive coupon

## 2.3 Pull-out tests

A direct screw withdrawal test of an Evolution Wingtip self-tapping screw with a diameter of 4.2 mm, a length of 38 mm and a thread pitch of 1 mm was conducted according to [12]. The screw was placed at the face of the panel (Figure 3) and connected the CSB to the flange of an LGS stud. The thickness of the CSB was 12 mm, while the LGS stud had a thickness of 1.2 mm. This configuration was identical to that used in practical applications.

According to EN 1993-1-3 [14], the capacity of the connection was expected to be:

$$F_{o,Rd} = \frac{0.65\ d\ t_{sup}\ f_{u,sup}}{\gamma_{M2}} = 1.21kN \quad (1)$$

where d is the diameter of the screw, $t_{sup}$ is the thickness of the supporting element (the stud), and $f_{u,sup}$ is the tensile strength of the supporting element. Two scenarios were studied: 1. Pull-out of the screw from both the CSB and the stud, and 2. Pull-out of the screw together with the CSB from the stud (i.e. the screw remains embedded in the CSB and the CSB does not contribute to the pull-out resistance). Therefore, a total of eleven specimens were tested – three with a screw connected to the bare LGS, and the rest with a screw connecting the CSB to the LGS. A constant displacement rate of 0.50 mm/min was applied until failure of the connection. The displacement of the actuator was recorded and taken as the displacement of the screw.

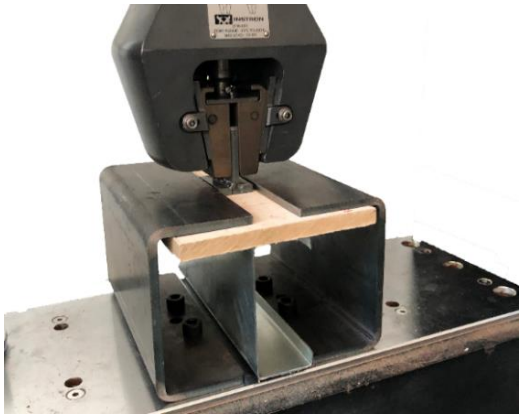

**Figure 3 -** Pull-out: experimental set-up

## 2.4 Push-out tests

The load-slip response of the screws under shear loading was recorded in a series of monotonic and cyclic push-out tests. Each specimen consisted of a LGS stud with a CSB panel screwed onto each of the flanges using self-tapping screws identical in geometry to the ones used for the pull-out experiment and taken from the same batch. These screws were provided at 300 mm spacings, as is common practice in residential LGS framed construction. The test setup was identical for both the monotonic and cyclic experiments and comprised of a 470 mm long LGS stud, two 12 mm thick CSB panels measuring 150 mm in width and 450 mm in height, and four self-tapping screws, as illustrated in Figure 4 (a). The load was applied through an Instron 8800 servo-hydraulic jack with a capacity of 250 kN. The loading protocol for the monotonic experiments was based on BS EN 383 [15]. The specimens were subjected to an initial loading cycle up to 40% of their expected capacity. Then, a load reversal was applied until the specimen had reverted to 10% of the expected ultimate load. Subsequently, the specimen was loaded to failure at a displacement rate of 1 mm/min. The same procedure was applied to all four specimens.

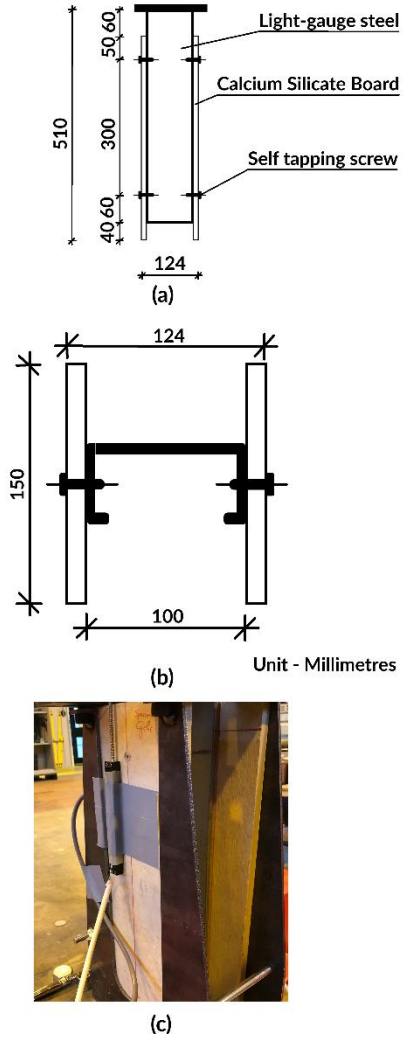


**Figure 4 -** Push-out experiment: (a) specimen elevation view, (b) specimen top view, (c) set-up

As cyclic loading, in the form of wind and earthquakes, results in load reversal, it is crucial to study effects such as pinching, caused by the enlargement the screw hole due to damage to its edge [16]. Therefore, the cyclic loading protocol proposed in [17] and illustrated in 4 was applied to a total of four specimens. The maximum displacement amplitude Δ in this protocol was derived from the results obtained in the monotonic experiments and was taken equal to the displacement $\Delta_m$ where the load had dropped below 80% of the peak load. The displacement rate was kept constant during the entirety of the test. The frequency of the loading was 0.20 Hz, while the amplitude gradually increased.

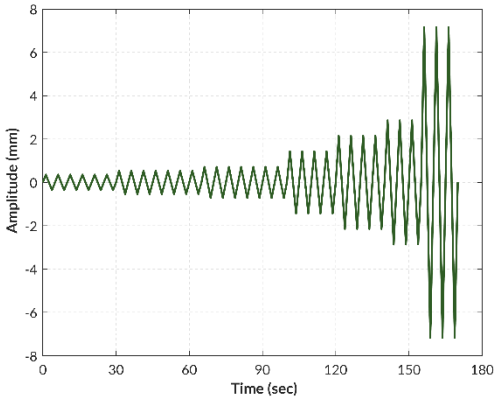


**Figure 5 -** Cyclic loading protocol for push-out test

## 3 Results & Discussion

### 3.1 Material test results

The results of the six cold-formed steel coupons are presented in Table 1, which lists the Young's modulus ($E$), yield stress ($f_y$), ultimate strength ($f_u$), peak strain ($\varepsilon_u$) and strain at fracture ($\varepsilon_f$). The label used to identify the coupons starts with the acronym for the material (LGS), followed by a letter indicating the location where the coupon was extracted (i.e. S for sheet, W for web of the stud, and F for flange of the stud). The specimens exhibited an average yield strength of 447.2 MPa, an ultimate strength of 595.6 MPa, a Young's modulus of 193 GPa and an elongation of 20% at fracture. As an indicative example, the engineering stress-strain curve for specimen LGS-W2 presented in Figure 6. The 'static' curve in this figure was obtained by reducing the stress values to be consistent with the levels observed during the pauses in loading.

**Table 1** - Cold formed steel: mechanical properties

| | $E$ (GPa) | $f_y$ (MPa) | $f_u$ (MPa) | $\varepsilon_u$ (%) | $\varepsilon_f$ (%) |
|---|---|---|---|---|---|
| **LGS-S1** | 195.2 | 423.5 | 586.1 | 13.2 | 18.0 |
| **LGS-S2** | 194.9 | 469.9 | 615.9 | 13.4 | 22.4 |
| **LGS-W1** | 190.7 | 437.8 | 590.3 | 13.7 | 20.5 |
| **LGS-W2** | 191.4 | 449.5 | 598.0 | 14.1 | 20.2 |
| **LGS-F1** | 192.0 | 451.3 | 599.6 | 13.3 | 18.2 |
| **LGS-F2** | 193.1 | 451.1 | 583.7 | 13.6 | 20.5 |
| **Avg.** | 192.9 | 447.2 | 595.6 | 13.6 | 20.0 |

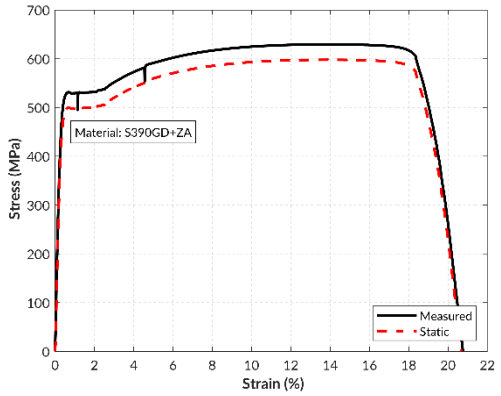


**Figure 6** – Cold formed steel: stress-strain curve for LGS-W2

The tensile and compressive stress-strain curves derived from the CSB coupons are presented in Figures 7-9. Tables 2-4 summarise the measured values of the tensile Young's Modulus ($E_{t,p}$), the ultimate tensile strength ($f_{t,p}$), the compressive Young's Modulus in the plane parallel to the surface ($E_{c,p}$), the ultimate compressive strength in the plane parallel to the surface ($f_{c,p}$), the compressive Young's Modulus in the direction normal to the surface ($E_{c,n}$), and the compressive strength at 5% deformation of the board thickness in the direction normal to the surface ($f_{c,n}$). It is clear from these values that the Young's modulus and ultimate strength differ depending on the direction of the loading, with the highest compressive strength observed in the direction normal to the surface. The CSB coupons subjected to compression parallel to the surface displayed 45-degree shear cracks during failure, as shown in Figure 7a, while the CSB coupons subjected to tension had their failure plane perpendicular to the loading in the middle of the gauge length.

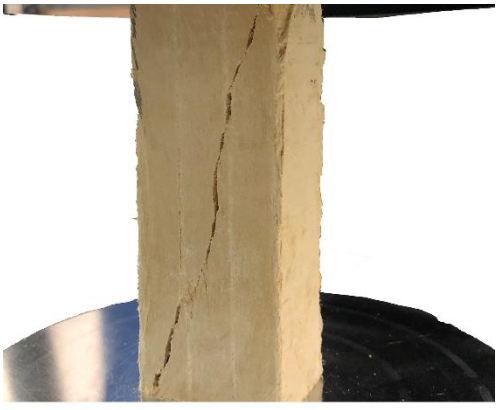

(a)

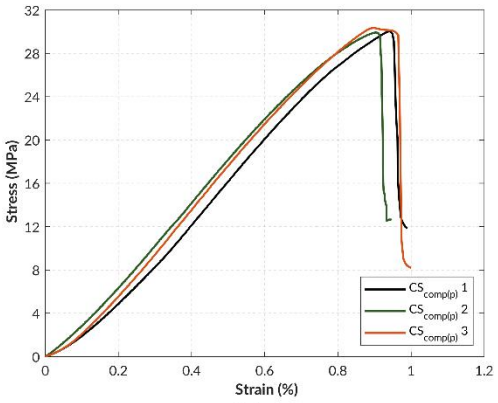


(b)

**Figure 7** – Calcium Silicate compressive coupon parallel to the surface: (a) failure mode, (b) stress-strain curve

**Table 2** – Calcium Silicate coupons: compressive properties parallel to surface

| | $E_{c,p}$ (GPa) | $f_{c,p}$ (MPa) |
|---|---|---|
| **$CS_{comp(p)}$ 1** | 3.7 | 30.0 |
| **$CS_{comp(p)}$ 2** | 3.8 | 29.9 |
| **$CS_{comp(p)}$ 3** | 3.9 | 30.4 |
| **Avg.** | 3.8 | 30.1 |

**Table 3** – Calcium Silicate coupons: compressive properties normal to surface

| | $E_{c,n}$ (GPa) | $f_{c,n}$ (MPa) |
|---|---|---|
| **$CS_{comp(n)}$ 1** | 1.3 | 63.7 |
| **$CS_{comp(n)}$ 2** | 1.4 | 60.0 |
| **$CS_{comp(n)}$ 3** | 1.4 | 60.4 |
| **Avg.** | 1.3 | 61.4 |

**Table 4** – Calcium Silicate coupons: tensile properties parallel to surface

| | $E_{t,p}$ (GPa) | $f_{t,p}$ (MPa) |
|---|---|---|
| **$CS_{tens(p)}$ 1** | 9.9 | 6.0 |
| **$CS_{tens(p)}$ 2** | 10.1 | 6.1 |
| **Avg.** | 10.0 | 6.1 |

(a)

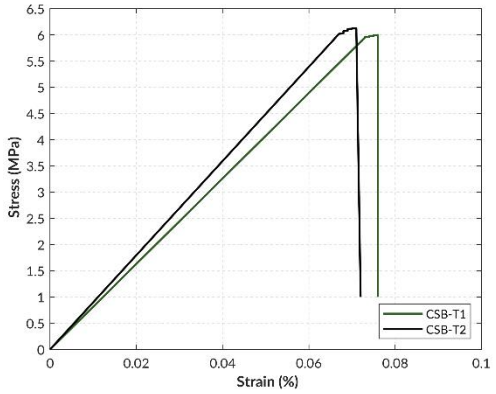


(b)

**Figure 8 –** Calcium Silicate tensile coupon: (a) failed specimen, (b) stress-strain curve

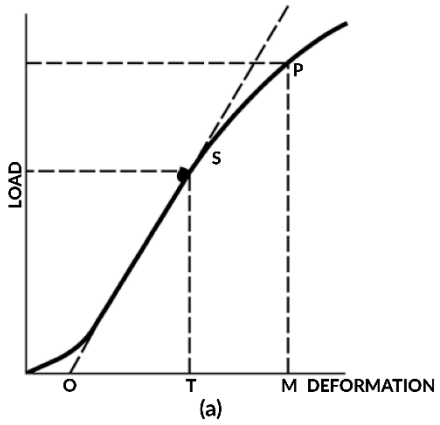


(a)

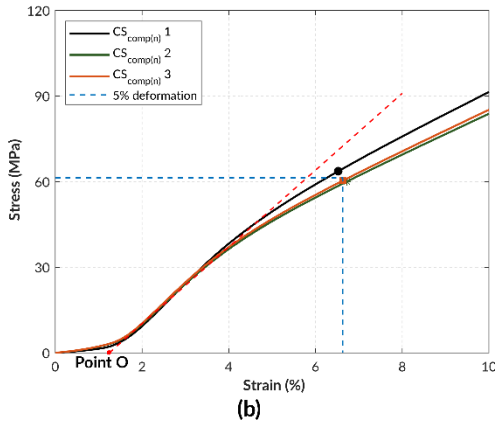


(b)

**Figure 9 –** Calcium Silicate compression in the direction normal to the surface: (a) calculation process from Procedure A [13], (b) experimental stress-strain curve

### 3.2 Pull-out test results

During the pull-out experiments, two failure modes were observed. The first failure mode (FM1) consisted of a loss of thread engagement due to localized damage to the thread. This caused a momentary drop in the force-displacement curve (Figure 10) until the next winding of the thread engaged with the stud material. In the second failure mode (FM2) the screw did not sustain any damage, rather pull-out was due to failure of the material the screw was embedded in (i.e. the CSB and LGS in the composite connection, or the LGS in the case of the bare steel connection). This failure mode consistently occurred at a displacement of about 3.5mm. The ultimate load was consistent between FM1 and FM2 in the CSB-LGS connection, with an average value of 3.95 kN. These capacities were more than 100% higher than the ones observed for the bare LGS-screw connection, which highlights the contribution of the CSB in the pull-out resistance. It also explains why FM1 was not observed in the bare steel connection. The average capacity of this connection was 1.95 kN, which is 60% higher than the value predicted by Eurocode 3 [14] (Eq. 1).and, again, for an ultimate displacement of about 3.5 mm.

**Table 5 -** Pull-out experiments: specimen capacities and failure modes

| | $P_{max}$ (kN) | Failure Mode |
|---|---|---|
| **P2** | 4.10 | FM1 |
| **P5** | 4.07 | FM1 |
| **P7** | 3.82 | FM1 |
| **P8** | 4.08 | FM1 |
| **Avg.** | 4.02 | - |
| **P1** | 4.16 | FM2 |
| **P3** | 3.96 | FM2 |
| **P4** | 3.31 | FM2 |
| **P6** | 4.06 | FM2 |
| **Avg.** | 3.87 | - |
| **B1** | 1.90 | FM2 |
| **B2** | 2.20 | FM2 |
| **B3** | 1.75 | FM2 |
| **Avg.** | 1.95 | - |

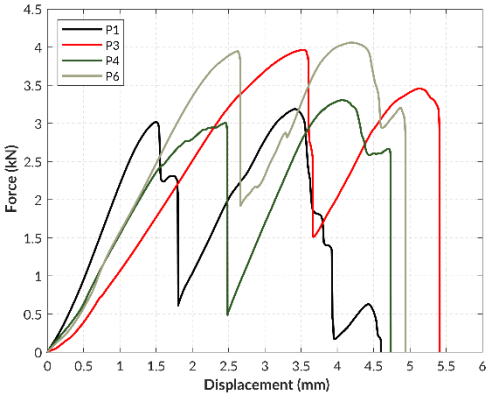


**Figure 10 -** Pull-out experiments: Results for Failure Mode 1

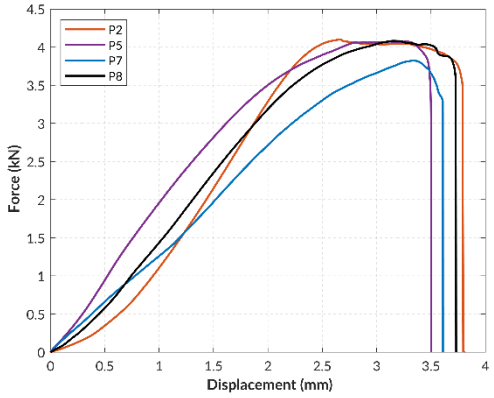


**Figure 11 -** Pull-out experiments: Results for Failure Mode 2

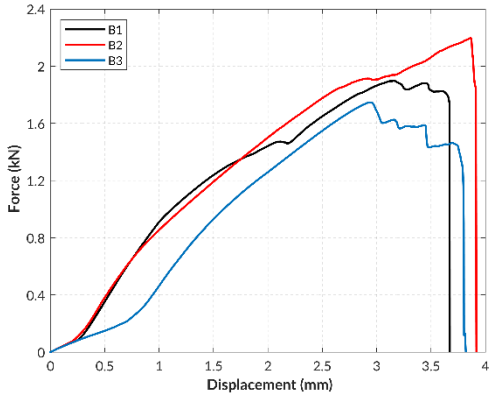


**Figure 12 -** Pull-out experiments: Results for bare steel connection

### 3.3 Push-out test results

The experimental observations in the push-out tests included localized damage to the CSB as a result of the screw bearing up against it (Figure 13b) and gradual tilting of the screws with an increase in slip (Figure 13a). The measured force-slip responses of the test specimens are illustrated in Figure 13. Based on [18], the ductility of the connection for each specimen was calculated through the following equation:

$$D = \frac{V_u}{V_y} \tag{2}$$

where $V_u$ and $V_y$ are the slip values corresponding to the ultimate load and the yield load, respectively. A summary of the experimental data corresponding to each specimen is presented in Table 6, including the ductility ($D$) of the connection, the maximum load per screw ($F_u$), the yield load per screw ($F_y$), the corresponding slip at maximum load ($V_u$) and the initial stiffness of the connection ($K_0$), calculated as the initial slope of the force-slip curve.

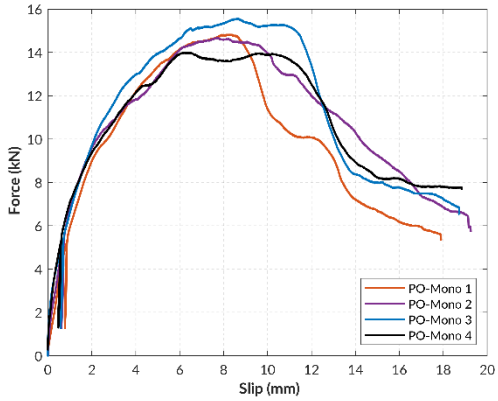


**Figure 13 –** Monotonic push-out experiment: Force-slip curves per specimen

As can be seen in Table 6, substantial ductility was achieved in the connection between LGS and CSB using self-tapping screws, allowing for sufficient redistribution of forces. The average ultimate capacity was 3.7 kN per screw and the corresponding average slip was 7.6 mm. The average stiffness of the connection ($K_o$) and the ductility ($D$) were 998.0 N/mm and 3.5, respectively.

**Table 6 -** Monotonic push-out test: Experimental results per screw

| | $F_u$ (kN) | $F_y$ (kN) | $V_u$ (mm) | $K_0$ (N/mm) | $D$ |
|---|---|---|---|---|---|
| **PO-Mono 1** | 3.7 | 2.4 | 7.9 | 976 | 3.5 |
| **PO-Mono 2** | 3.7 | 2.5 | 7.7 | 978 | 3.3 |
| **PO-Mono 3** | 3.9 | 2.6 | 8.6 | 977 | 3.7 |
| **PO-Mono 4** | 3.5 | 2.3 | 6.3 | 1062 | 3.4 |
| **Avg.** | 3.7 | 2.5 | 7.6 | 998 | 3.5 |

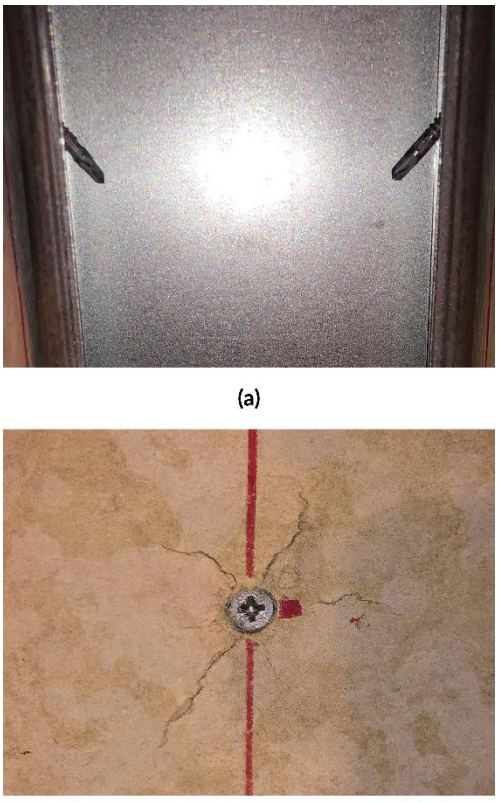

**(a)** **(b)**

**Figure 14 -** Push-out experiment: (a) tilting of the screw, (b) bearing failure of CSB

The specimens subjected to cyclic excitations presented identical failure modes, i.e. bearing of the screw onto the board and tilting of the screw. A distinct pinching behaviour was observed in the hysteresis loop in both directions of loading. This was a result of irreversible deformations in the bearing interface between the CSB and the screw and a consequent enlargement of the hole. This behaviour is illustrated in Figure 15 for the first specimen, while the envelope curves of all the specimens are presented in Figure 16.

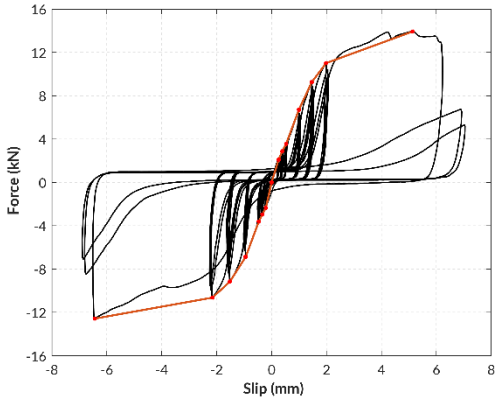


**Figure 15** - Cyclic push-out test: Force-slip curve for specimen PO-Cyclic 1

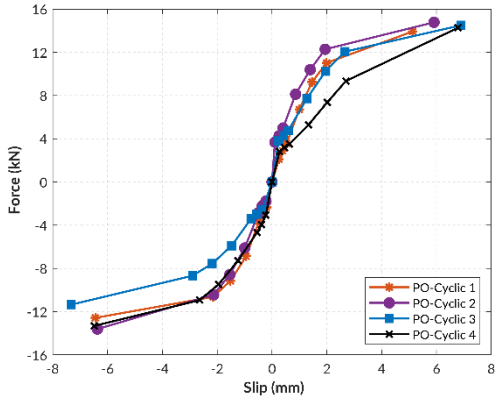


**Figure 16** - Cyclic push-out tests: Envelope curves

## 4 Conclusions

A series of experiments were carried out to investigate the behaviour of self-tapping screws used in construction practice to connect CSB to LGS studs. The properties of these latter two materials were investigated through a number of standardized tests, while pull-out and push-out experiments were executed to determine the capacity of the connection.

Direct pull-out tests were carried out to determine the pull-out resistance of (1) the screw from the LGS stud, and (2) the screw from both the CSB and the LGS. It was found that the capacity was higher in the latter case by a factor of 2, reflecting the added influence of the boards. Two failure modes were observed in the latter case: failure of the screw thread and failure of the surrounding material. Failure of the screw threads was absent in the former case. The screw capacity significantly exceeded the Eurocode 3 prediction.

The shear behaviour of the connectors was investigated through four monotonic and four cyclic push-out tests. Failure was observed in both cases to originate from tilting of the screws and bearing failure in the CSB. The connection displayed significant pinching behaviour under cyclic loading. The cyclic backbone curve showed good agreement with the monotonic curve. The ultimate shear force resisted by each screw was 3.7 kN on average, with a peak displacement of about 7.6 mm.

In a next stage of the research, the material properties and connector behaviour obtained in this study will serve as input for detailed finite element models, with the aim of studying the composite action between the CSB and the LGS studs in wall panels under in-plane lateral loads. Accounting for this composite diaphragm action through safe and accurate design rules would have definite benefits for construction efficiency and material use.

## 5 Acknowledgements

This project was funded by the Construction Scotland Innovation Centre through the i-Con Challenge fund. The authors would like to acknowledge the contribution of Mr Richard Webb of Newton Steel Framing for providing the necessary material for completing the experimental program. The authors would also like to thank Mr Mark Partington and Mr Jim Hutcheson at the University of Edinburgh – School of Engineering for their assistance in specimen preparation and testing.

## References

[1] B. W. Schafer, “Cold-formed steel structures around the world,” *Steel Constr.*, vol. 4, no. 3, pp. 141-149[1] B. W. Schafer, “Cold-formed steel struc, 2011, doi: 10.1002/stco.201110019.

[2] M. R. Javaheri-Tafti, H. R. Ronagh, F. Behnamfar, and P. Memarzadeh, “An experimental investigation on the seismic behavior of cold-formed steel walls sheathed by thin steel plates,” *Thin-Walled Struct.*, vol. 80, pp. 66–79, 2014, doi: 10.1016/j.tws.2014.02.018.

[3] K. Roy, H. H. Lau, T. C. Huon Ting, R. Masood, A. Kumar, and J. B. P. Lim, “Experiments and finite element modelling of screw pattern of self-drilling screw connections for high strength cold-formed steel,” *Thin-Walled Struct.*, vol. 145, no. July, p. 106393, 2019, doi: 10.1016/j.tws.2019.106393.

[4] C. Blais and C. A. Rogers, “Testing and design of light gauge steel frame / 9 mm OSB panel shear walls,” *Eighteenth Int. Spec. Conf. Cold-Formed Steel Struct. Recent Res. Dev. Cold-Formed Steel Des. Constr.*, vol. 2006, pp. 637–662, 2006.

[5] J. Ye, X. Wang, and M. Zhao, “Experimental study on shear behavior of screw connections in CFS sheathing,” *J. Constr. Steel Res.*, vol. 121, pp. 1–12, 2016, doi: 10.1016/j.jcsr.2015.12.027.

[6] P. Kyvelou, L. Gardner, and D. A. Nethercot, “Testing and Analysis of Composite Cold-Formed Steel and Wood-Based Flooring Systems,” *J. Struct. Eng. (United States)*, vol. 143, no. 11, pp. 1–16, 2017, doi: 10.1061/(ASCE)ST.1943-541X.0001885.

[7] V. Macillo, L. Fiorino, and R. Landolfo, “Seismic response of CFS shear walls sheathed with nailed gypsum panels: Experimental tests,” *Thin-Walled Struct.*, vol. 120, no. August, pp. 161–171, 2017, doi: 10.1016/j.tws.2017.08.022.

[8] J. Ye and X. Wang, “Piecewise function hysteretic model for cold-formed steel shear walls with reinforced end studs,” *Appl. Sci.*, vol. 7, no. 1, 2017, doi: 10.3390/app7010094.

[9] R. Serrette and D. Peyton, “Strength of Screw Connections in Cold-Formed Steel Construction,” *J. Struct. Eng.*, vol. 135, no. 8, pp. 951–958, Aug. 2009, doi: 10.1061/(ASCE)0733-9445(2009)135:8(951).

[10] British Standards Institution BSI, *BS EN ISO 6892-1:2019 - Metallic materials - Tensile testing*. British Standards Institution BSI, 2019.

[11] Y. Huang and B. Young, “The art of coupon tests,” *J. Constr. Steel Res.*, vol. 96, pp. 159–175, 2014, doi: 10.1016/j.jcsr.2014.01.010.

[12] ASTM International, *D1037-12 - Standard test methods for evaluating Properties of Wood-Based Fiber and Particle Panel Materials*. West Conshohocken, PA: ASTM International, 2012.

[13] ASTM International, *C165-07 (Reapproved 2017) - Standard*

*Test Method for Measuring Compressive Properties of Thermal Insulations*. West Conshohocken, PA: ASTM International, 2017.

[14] British Standards Institution, "BS EN 1993-1-3:2006."

[15] British Standards Institution, "BS EN 383:2007 - Timber Structures - Test methods - Determination of embedment strength and foundation values for dowel type fasteners," 2007.

[16] J. Ye, X. Wang, H. Jia, and M. Zhao, "Cyclic performance of cold-formed steel shear walls sheathed with double-layer wallboards on both sides," *Thin-Walled Struct.*, vol. 92, pp. 146–159, 2015, doi: 10.1016/j.tws.2015.03.005.

[17] H. Krawinkler, F. Parisi, L. Ibarra, A. Ayoub, and R. Medina, "Development of a Testing Protocol for Woodframe Structures," *CUREE - Caltech Woodframe Proj.*, pp. 1–76, 2001, [Online]. Available: https://www.curee.org/publications/woodframe/downloads.

[18] British Standards Institution, "BS EN 12512:2001 - Timber structures - test methods - cyclic testing of joints made with mechanical fasteners [including amendment A1:2005]," 2005.